CHAPTER II

SPACECRAFT

By Charles T. D'Aiutolo
NASA Headquarters

SECTION I - DESCRIPTION

The micrometeoroid satellite Explorer XIII was the payload of Scout vehicle ST-6, and contained five experiments to obtain information regarding micrometeoroids. These experiments consisted of the following detectors: pressurized cells, steel-covered grids, copper-wire cards, cadmium-sulfide cells, and impact detectors. In addition, a series of temperature measurements were made at selected places throughout the satellite. Voltage measurements were made on test solar cells to measure degradation of the cells.

Configuration.- The satellite was cylindrical in shape; about 23 inches in diameter and about 76 inches in length. The general arrangement of the spacecraft is shown in figure II-1, and exploded views are shown in figure II-2. The satellite was installed around the fourth stage of the Scout vehicle (X-248 rocket motor). The Langley pressurized-cell experiment was mounted around the periphery of the rocket motor; the Lewis steel-covered-grid experiment and the Goddard copper-wire-card experiment were located on the fourth-stage support structure. A shell was mounted on the fore-end of the spacecraft just forward

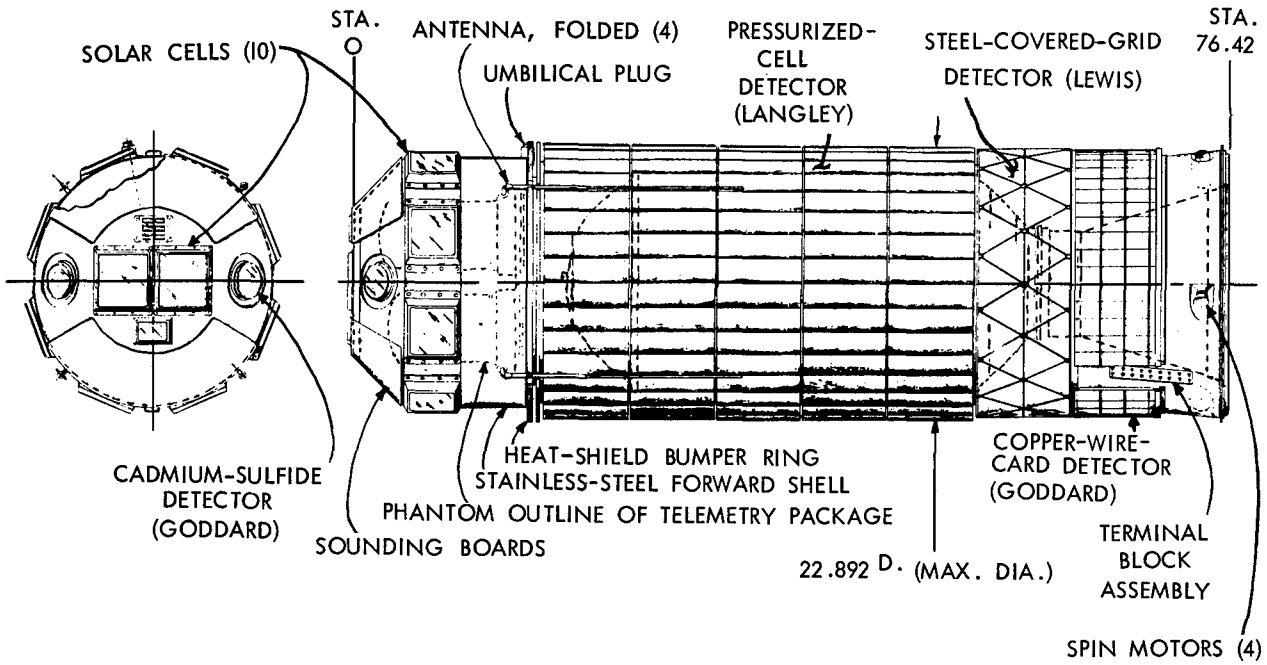

Figure II-1.- General arrangement of Explorer XIII.

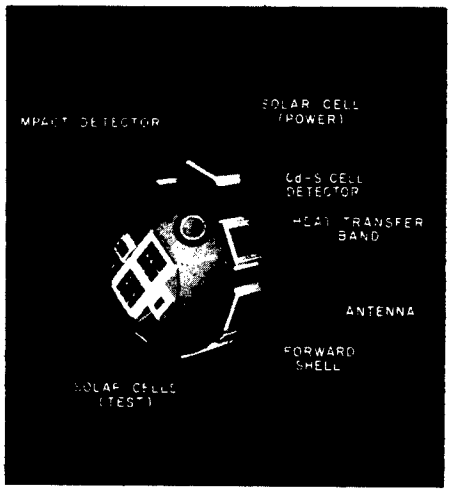

FORWARD SECTION

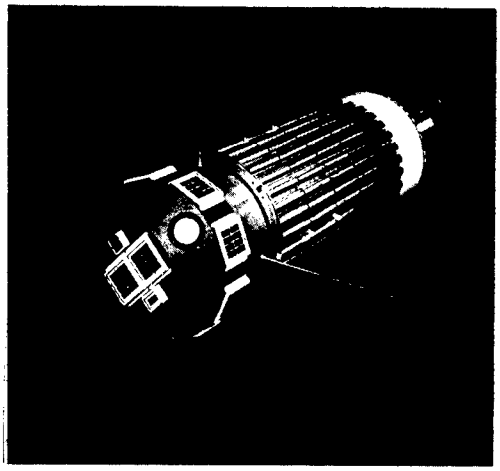

ASSEMBLED SPACECRAFT

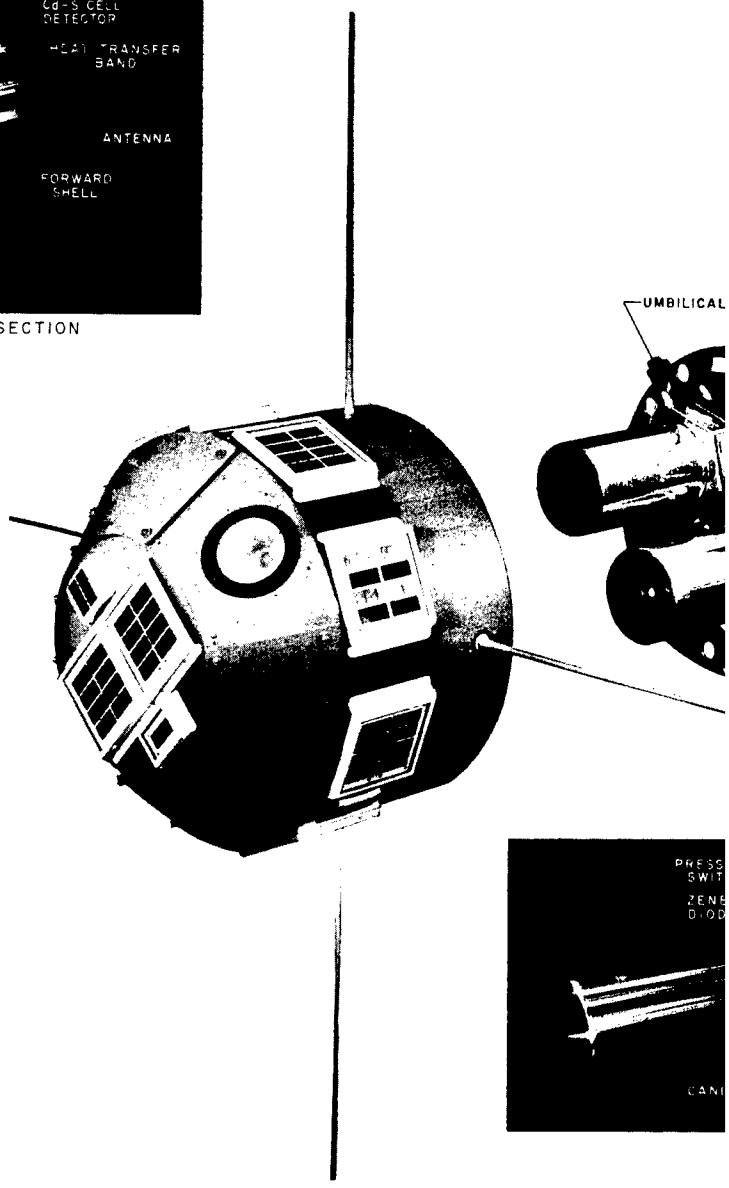

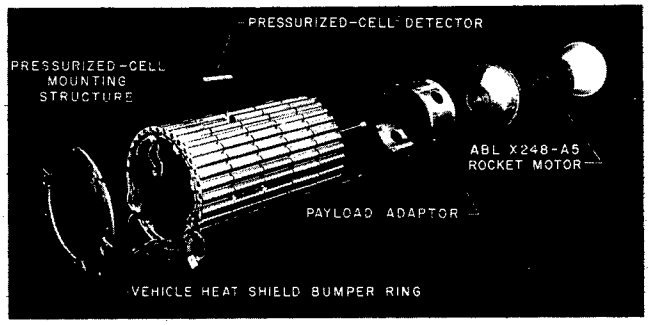

CENTER SECTION

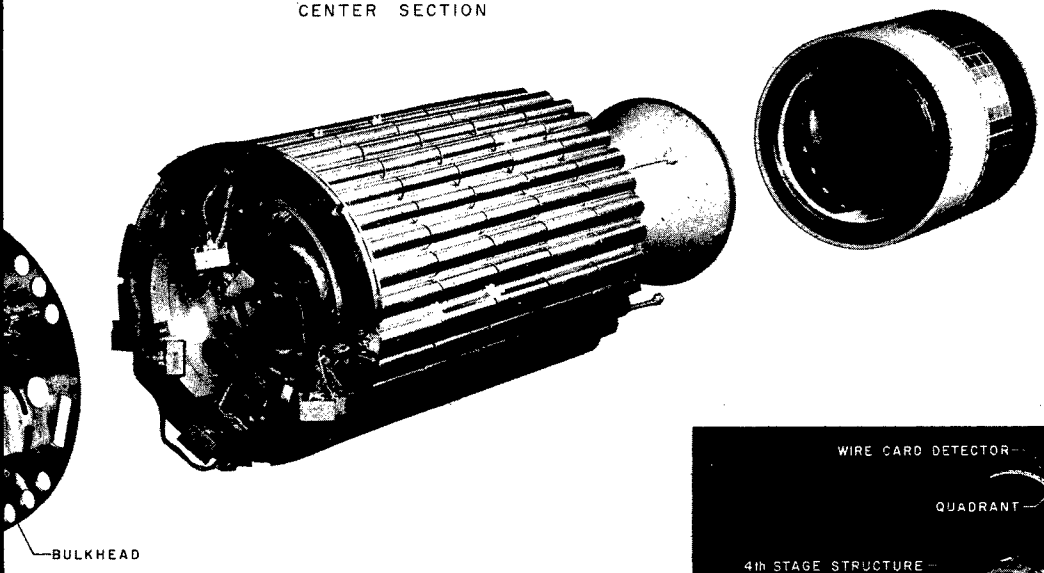

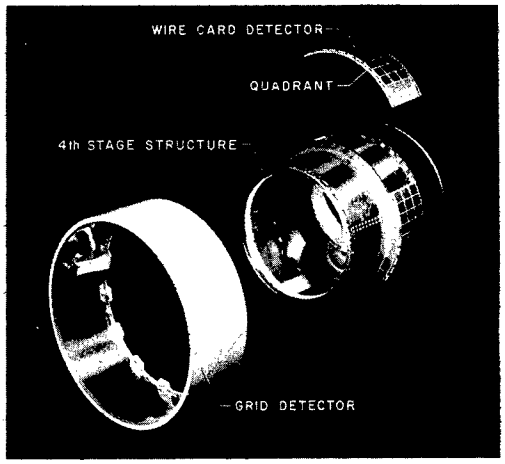

AFT SECTION

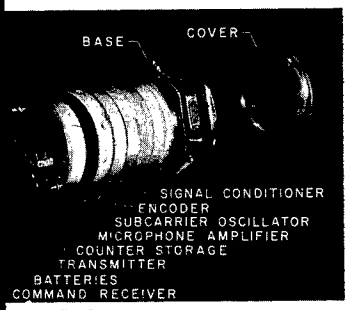

TELEMETER

Figure II-2.- Exploded view of Explorer XIII. L-64-3017

of the pressurized-cell experiment. On this shell were mounted the erectile antennas, the solar cells, the cadmium-sulfide cells, and "sounding boards" to which were mounted impact detectors to determine collisions with micrometeoroids. The "sounding boards" were acoustically isolated from the rest of the satellite structure. Within the shell and upon a thermally isolating bulkhead, were mounted the telemeters and the radio beacon. Detectors from each experiment were divided equally between the two telemeters. It should be noted that the motor casing is used as a structural member for the satellite and thus went into orbit as part of the satellite. A cutaway drawing of the satellite is presented in figure II-3 and shows the instrumentation telemeters and mounting details of solar cells and experiments as well as other features. A brief description of the experiments follows. More detailed descriptions are presented in later chapters and in reference III-1.

Langley Pressurized-Cell Detector.- The Langley pressurized-cell detectors are the primary sensors of the satellite and occupy the major portion of the sensitive area. A total of 160 cells of various thicknesses were mounted around the periphery of the spacecraft in five circular rows. Each row contained 32 cells. The cells were fabricated from beryllium-copper. Details of the pressurized-cell experiment are shown in figure II-4 and discussed in more detail in chapter IX. Five different thicknesses were incorporated: 0.001, 0.0015, 0.002, 0.0025, and 0.005 inch. The cells were pressurized with helium so that a puncture by a micrometeoroid would allow the helium to leak out. By means of a pressure-activated switch located on each cell, the pressure loss could be detected and telemetered. Helium gas was used in the cells and was pressurized to about 10 psi over atmospheric pressure so that the pressure switch would be closed on the ground, thereby providing a check prior to launch; the switch would open if the pressure in the cell dropped to about 5 psi. No attempt was made to monitor pressure leak rate. The penetration area of each detector is about 21.8 sq in. (140 cm^2) so that 24.2 sq ft (2.25 m^2) of area were exposed for this experiment. However, because of the semicircular cross section of the pressurized cells (see fig. II-4) the effective area for micrometeoroid capture was smaller than the exposed area. This effective area was considered to be π times the diameter of the outer surface (23 inches, see fig. II-1), multiplied by the detector sensing length of the column of five detectors (35.6 inches) with a correction for the open area between detectors. This definition of area gives a total value of 17 square feet (1.58 square meters).

Shown in the following table are the number of beryllium-copper cells of each thickness as well as the exposed area of each thickness:

Thickness, in.	Number of cells	Total exposed area in -	
		Sq ft	Sq m
0.0010	60	6.350	0.58
.0015	40	4.250	.40
.0020	20	2.125	.20
.0025	20	2.125	.20
.0050	20	2.125	.20

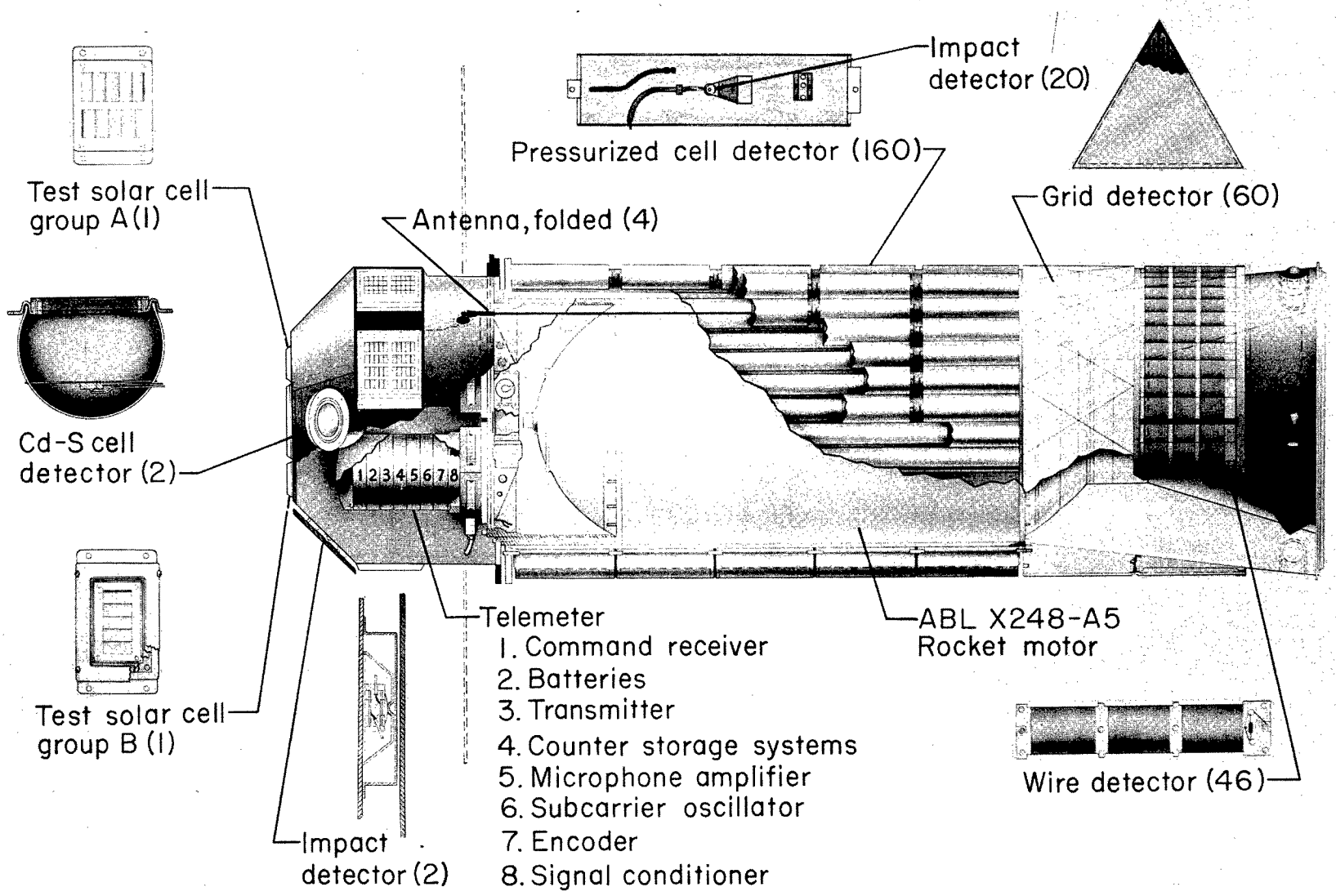

L-64-3076

Figure II-3.- Cutaway view of the micrometeoroid satellite.

Lewis Steel-Covered-Grid Detectors.- The Lewis steel-covered-grid detectors were units developed by the Lewis Research Center. A drawing of this detector is presented in figure II-5. Each detector consisted of a printed circuit about 60 microinches thick attached to 0.00025-inch-thick insulation. This circuit was mounted on the underside of type 304 stainless-steel skin samples. The samples were 0.003 and 0.006 inch thick. Each sample is an equilateral triangle whose sides are 4.57 inches long. The satellite incorporated 60 of these detectors. The thicknesses and areas are listed in the following table:

Thickness, in.	Number of sensors	Total exposed area in -	
		Sq ft	Sq m
0.003	50	3.00	0.28
.006	10	.75	.07

A detailed description of this experiment is given in reference II-1.

Goddard Copper-Wire-Card Detectors.- These copper-wire-card detectors were developed by the Goddard Space Flight Center and were similar to the detectors flown on the Explorer I as well as other satellites. A drawing of the

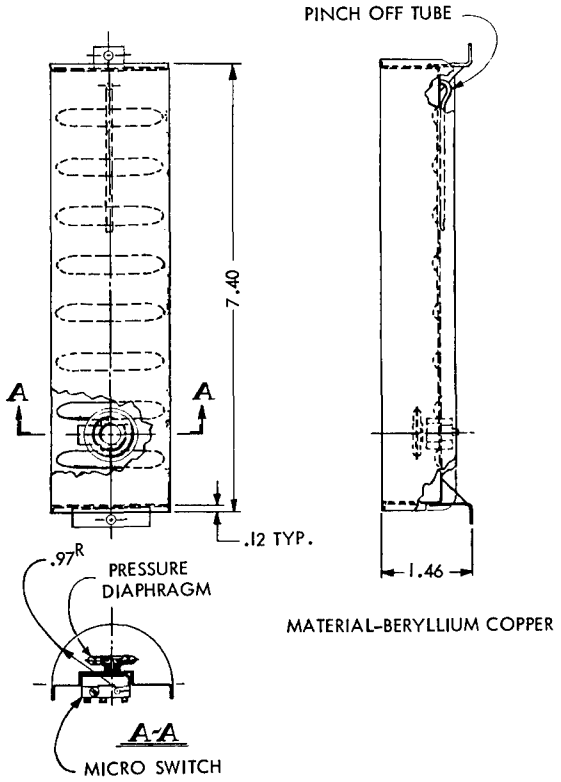

Figure II-4.- Pressurized-cell detector. All dimensions in inches.

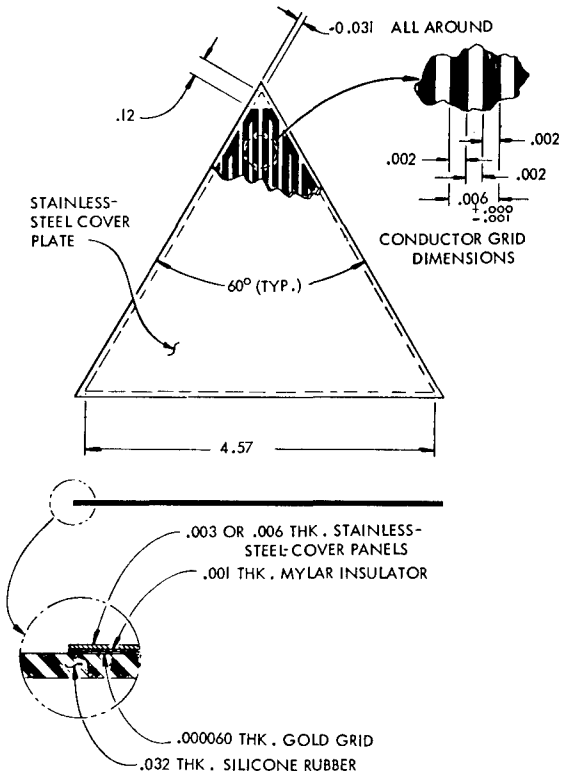

Figure II-5.- Steel-covered-grid detector. All dimensions in inches.

copper-wire-card detector is shown in figure II-6 and is discussed in detail in chapter X. Each detector consisted of a winding of fine wire mounted to a card

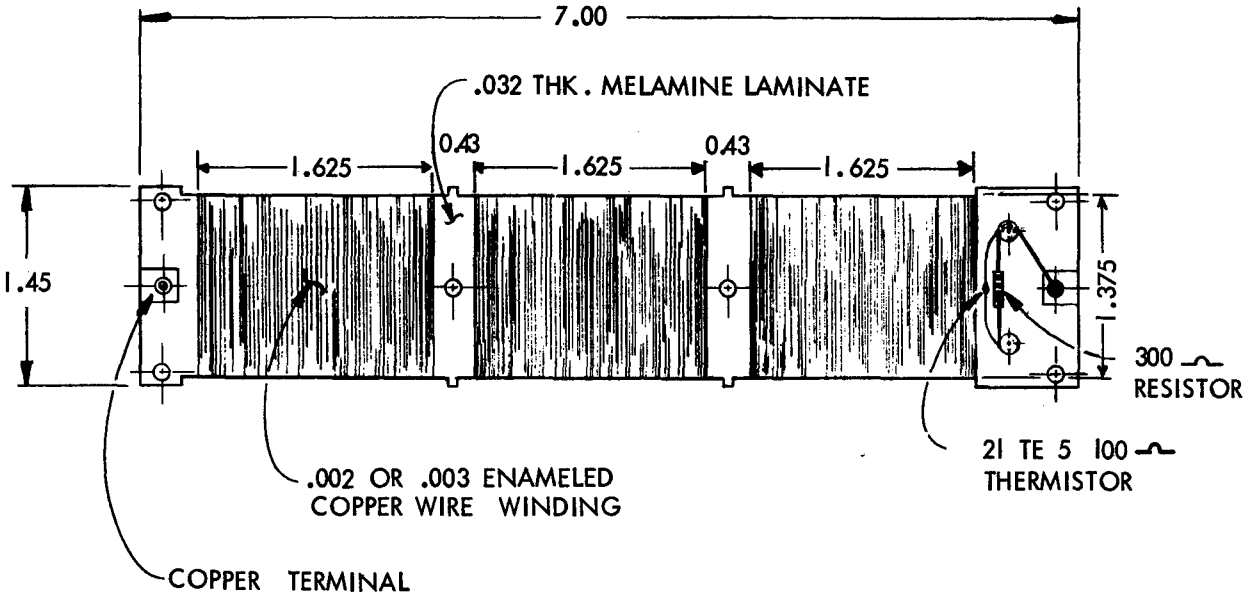

Figure II-6.- Copper-wire-card detector. All dimensions in inches.

rectangular in shape whose dimensions were 1.45 by 7.00 inches. This experiment incorporated two wire sizes of 0.002- and 0.003-inch diameter. Thicknesses and areas are shown in the following table:

Thickness, in.	Number of sensors	Total exposed area in -	
		Sq ft	Sq m
0.002	14	0.98	0.09
.003	32	2.27	.21

Goddard Cadmium-Sulfide Cells.- The cadmium-sulfide-cell detectors were also developed by the Goddard Space Flight Center. A drawing of this detector is shown in figure II-7 and discussed in detail in chapter XI. Basically, the detector consisted of a Cd-S cell mounted in an aluminum-coated glass flask. The exposed surface, whose diameter was about 2.6 inches (6.1 cm) (actual useful diameter about 2.00 inches (5.08 cm)), was covered with a sheet of 0.00025-inch film coated with evaporated aluminum on both sides. Extremely small particles could penetrate the aluminized film and allow light to enter the cell. The geometry of the flask was designed to focus the light onto the Cd-S cell; the cell resistance changed as a function of illumination. Two of these units were incorporated on the spacecraft, and were mounted in the forward shell, 180° apart. (See fig. II-1.)

Langley Impact Detectors.- The impact detectors were a Langley experiment and three levels of sensitivity were employed. Two acoustically isolated "sounding boards" on the forward shell were used for the highest and lowest levels, and twenty 0.005-inch pressurized cells were instrumented with transducers for the intermediate sensitivity level. Figures II-8 and II-9 are drawings of the impact detectors on the sounding boards and pressurized cells. This experiment is discussed in more detail in chapter XII. The following table lists the area and design sensitivities of the impact detectors.

Component	Total exposed area in -		Design sensitivity, dyne-sec
	Sq ft	Sq m	
Sounding boards	1.53	0.14	{ 1 .01
0.005-inch pressurized cells	2.30	.21	.1

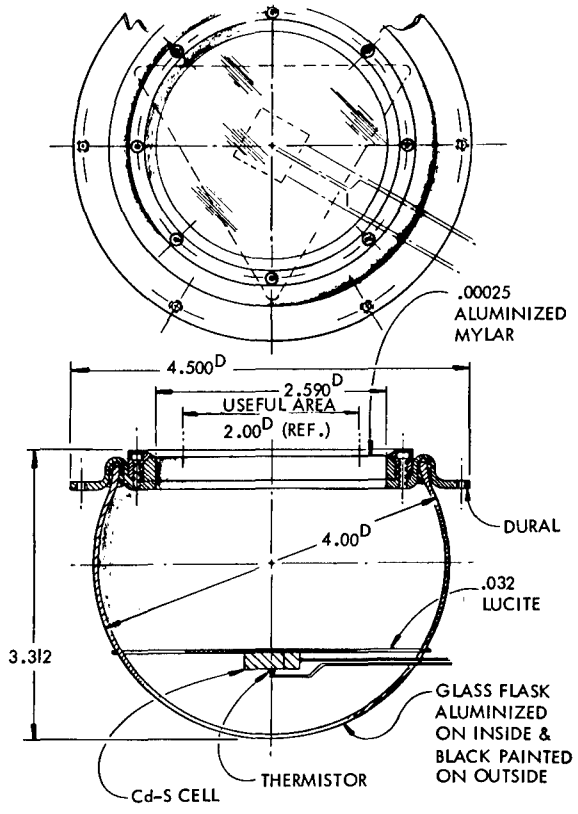

Figure II-7.- Cadmium-sulfide cell detector. All dimensions in inches.

Detector Correlation.- From the preceding discussion of the various penetration and impact experiments, it may be seen that each of the detectors complemented each other, thereby allowing a correlation to be made between the individual detectors.

The total exposed area of all penetration and impact detectors on the Explorer XIII was about an order of magnitude greater than other micrometeoroid experiments flown on earlier satellites.

Silicon Solar Cells.- These detectors were planned to determine the adverse effects of space environments on the silicon solar cells. There were five groups of five shingled solar cells; one group had 0.062 inch of fused silica mounted 0.062 inch above the cells, two groups had 0.006 inch of glass bonded directly to the solar cells with an epoxy cement, and the remaining two groups were unprotected. Three of the test solar cell groups were mounted to the front face of the forward shell. The remaining two test solar cell groups were mounted 180° apart on the cylindrical section of the forward shell.

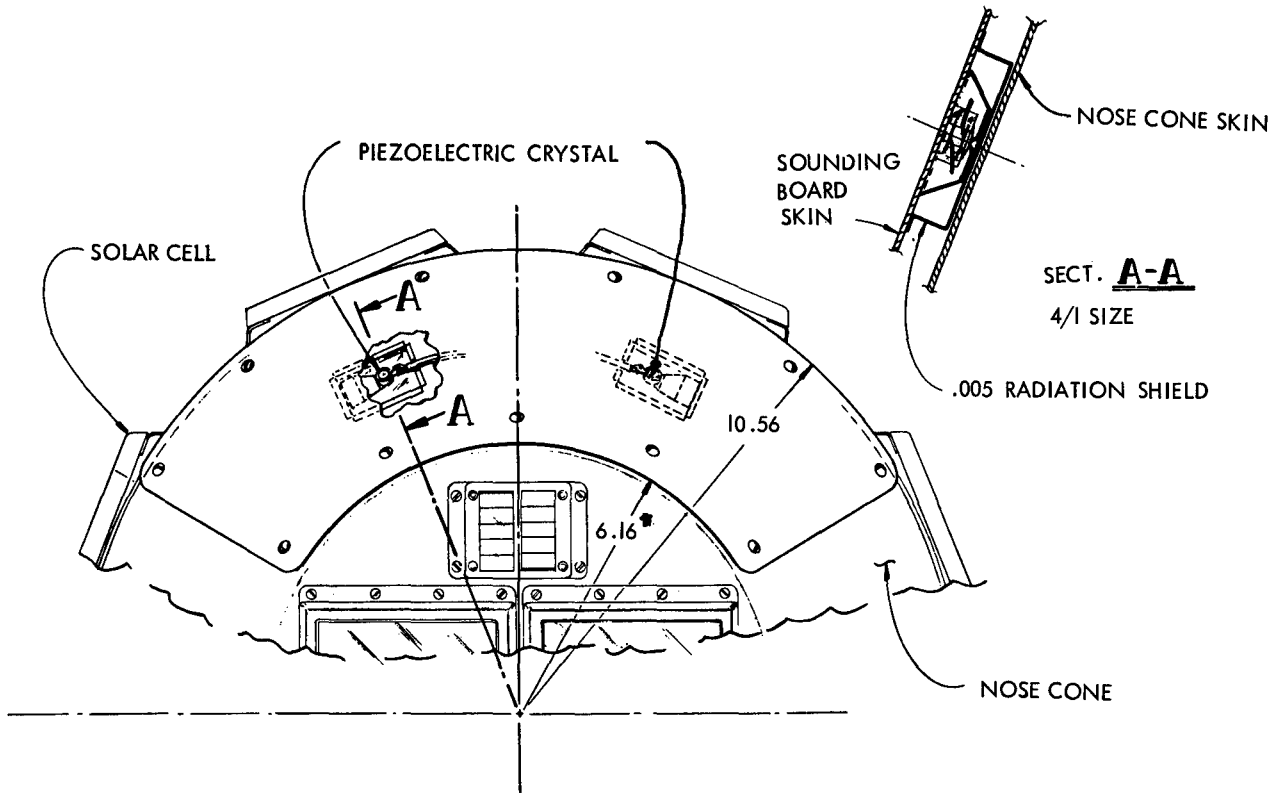

Figure II-8.- Sounding-board impact detectors. All dimensions in inches.

Sketches of the solar cell groups are shown in figures II-10 and II-11. Further description of this experiment appears in chapter V, section V.

Satellite Weight Breakdown.- The weight breakdown of the micrometeoroid satellite is shown in table II-1. Total payload weight including experiments, mounting hardware, telemeters, and support structure was 127.35 pounds. Weight of spent fourth-stage motor, spent spin rockets, as well as the upper "D" section of the Scout vehicle was 62.53 pounds so that the total weight in orbit was 189.88 pounds.

SECTION II - LAUNCH OPERATIONS

General Description of Launch Vehicle.- As stated in the previous section, the micrometeoroid satellite was the payload of Scout ST-6. Only a brief description of the Scout will be presented herein.

The Scout is a small launch vehicle capable of being used as a high-altitude probe, a reentry vehicle, or as a satellite launching vehicle. A general arrangement drawing of Scout, showing staging, is presented in figure II-12. The Scout is a four-stage, solid-propellant, rocket vehicle using a preprogramed control system for guidance. The first and second stages are steel-walled

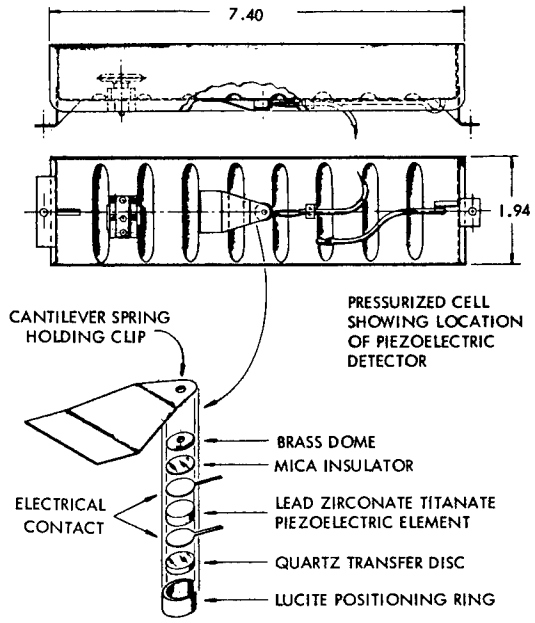

Figure II-9.- Impact detector mounted on pressurized cells. All dimensions in inches.

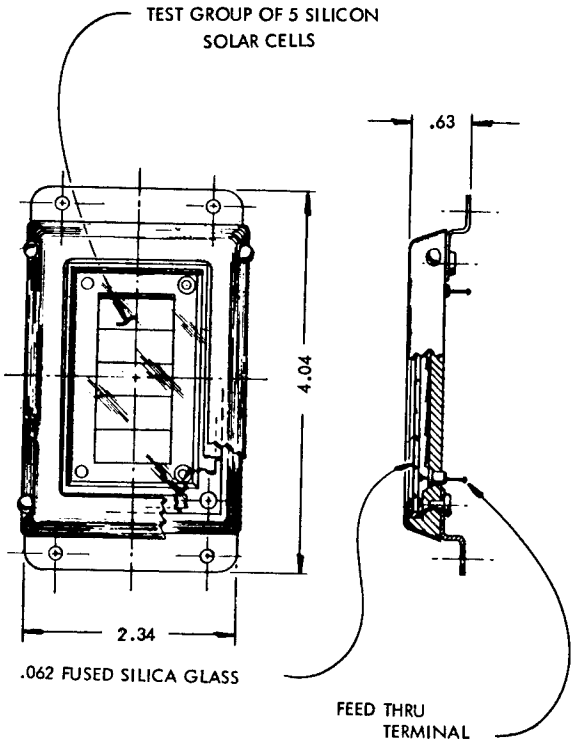

Figure II-10.- Single solar-cell test unit. All dimensions in inches.

vessels and the third and fourth stages are of fiber-glass construction. Heat-shield-drag fairings were placed around the third-stage rocket motor, the fourth stage, and the payload in order to protect these units during flight within the dense part of the atmosphere. Aerodynamic tip controls and jet vane controls are used for attitude control of the first stage and H_2O_2 control jets are used on the second and third stages for attitude control as the flight progresses. The vehicle is attitude controlled up to fourth-stage ignition and is spin stabilized through fourth-stage burning.

Preflight Operations.- After environmental tests, calibrations, and final checkouts as described in later chapters of this paper, the micrometeoroid satellite as well as the prototype satellite was shipped to the Wallops Station for launch preparations. The prototype satellite was used for fitting checks as

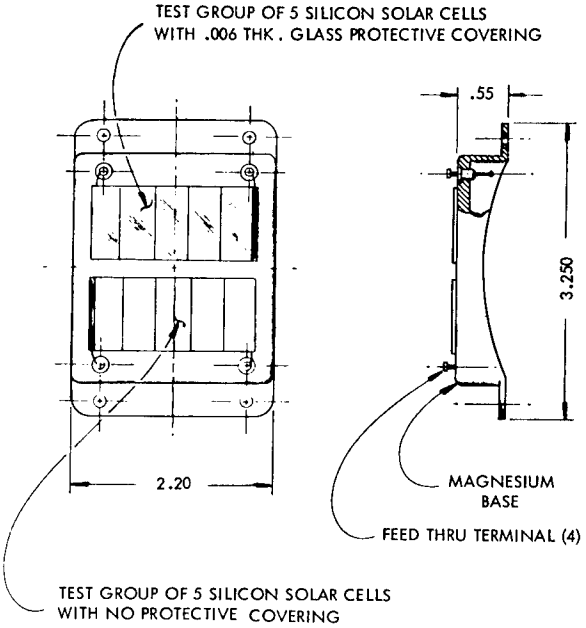

Figure II-11.- Double solar-cell test unit. All dimensions in inches.

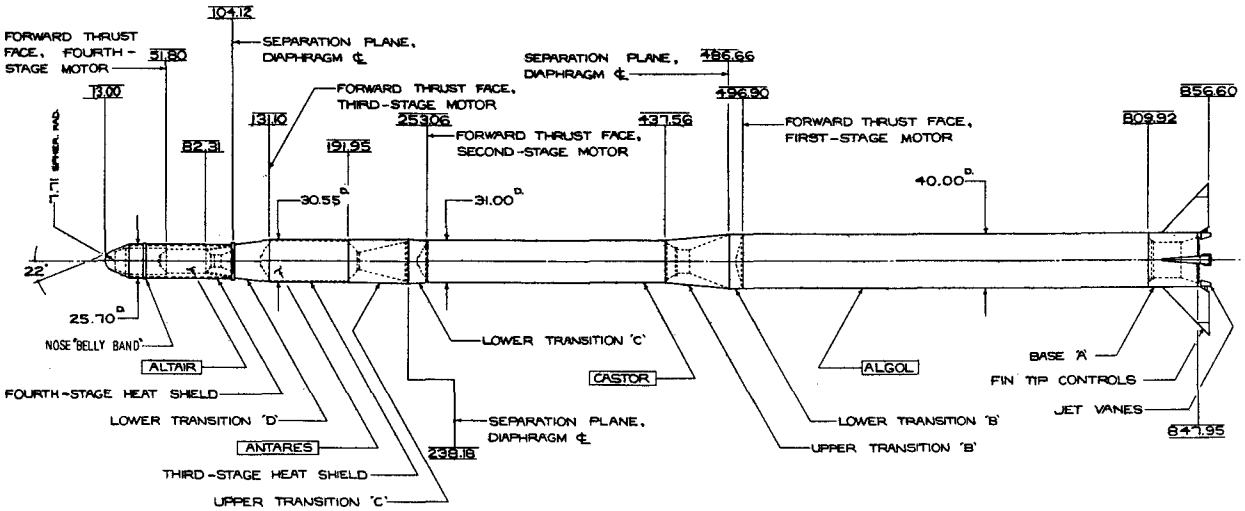

Figure II-12.- General arrangement of Scout vehicle. All dimensions in inches.

well as vehicle systems checks before the vehicle was assembled on the launch tower. A photograph of a vehicle-system check is shown in figure II-13.

Upon arrival at the launch facility, the micrometeoroid satellite underwent a performance check to ascertain that no damage occurred in shipment. The center of gravity of the payload with a spent fourth-stage rocket motor and a fourth-stage support structure attached was then determined (fig. II-14) so that final vehicle ascent characteristics could be ascertained. Next, the satellite was disassembled, moved to an explosion-proof room, and assembled around a live fourth-stage rocket motor. Alinement checks were made and the payload and the live fourth-stage motor with fourth-stage support structure attached were dynamically balanced (fig. II-15) to insure true spinning during fourth-stage burning. After dynamic balancing and extensive instrument checks and inspections, the satellite was placed within

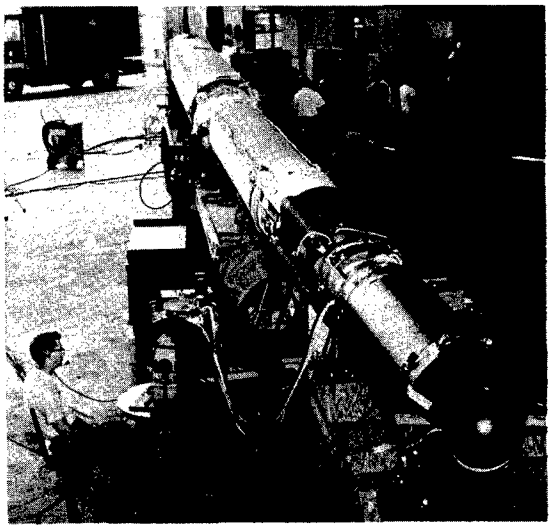

L-64-3077
Figure II-13.- Spacecraft-vehicle systems checks.

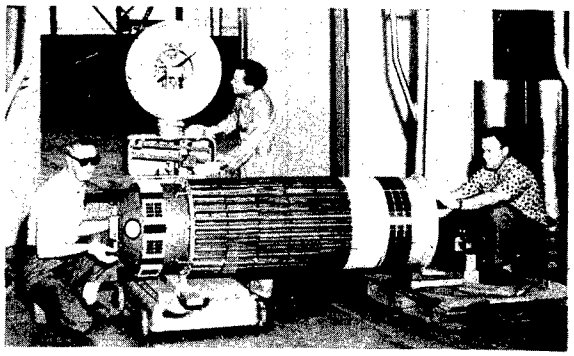

L-64-3078
Figure II-14.- Spacecraft center-of-gravity determination.

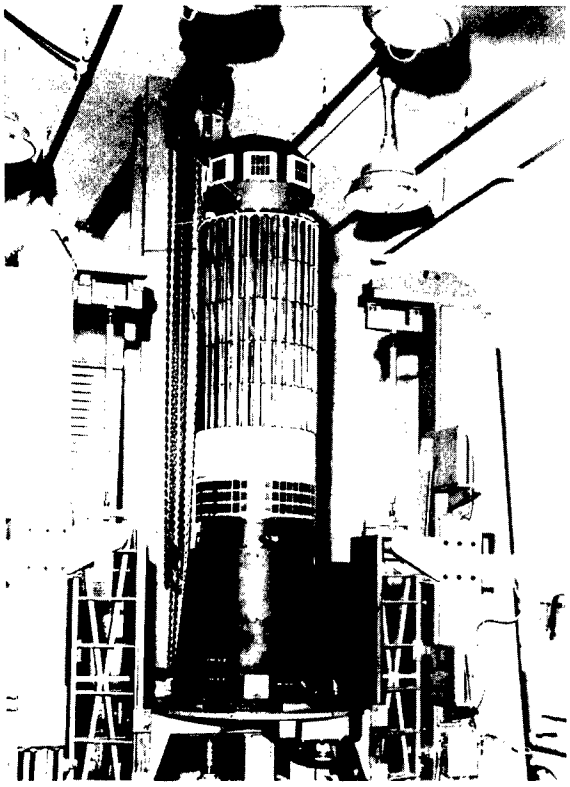

L-64-3079
Figure II-15.- Dynamic balancing of spacecraft.

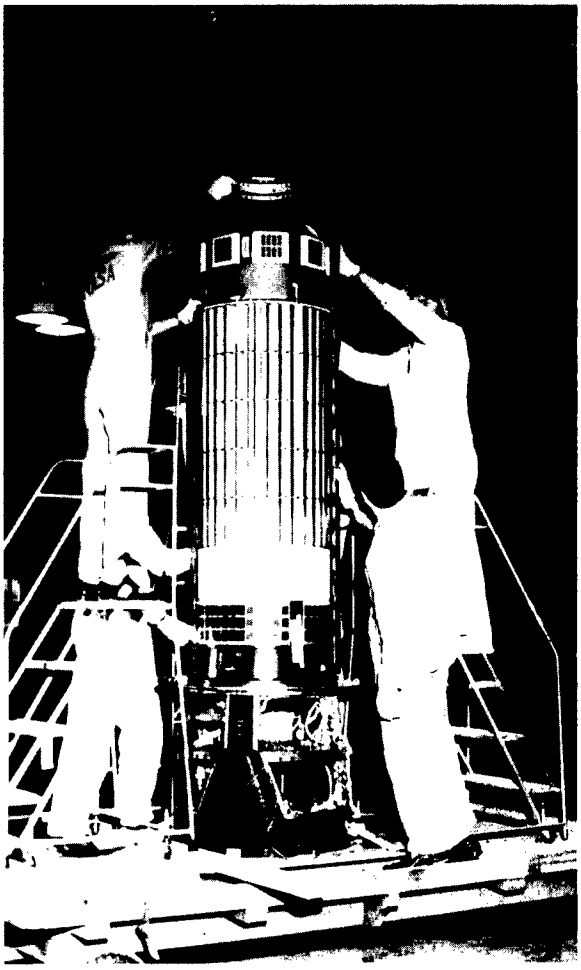

L-64-3080
(a) Within one-half of heat shield.

Figure II-16.- Spacecraft within Scout fourth-stage heat shield.

the fourth-stage payload heat shield (figs. II-16(a) and II-16(b)) and transported to the launch tower. At the tower, the fourth stage with payload attached and with heat shield in place was elevated (fig. II-17) and mated to the first three stages of the Scout launch vehicle (fig. II-18). Prior to launch, the satellite underwent a series of tests and checks including electrical tests, mutual interference checks between vehicle and payload, and payload final performance checks as well as payload calibrations before the start of the launch countdown. Prelaunch reference measurements were made on all experiments during the countdown just prior to lift-off. In lieu of a backup micrometeoroid satellite payload, backup components were available at the launch site in the event of a payload failure. It was not practical to have available a complete backup payload since the fourth-stage motor is contained within the payload and only one fourth-stage motor was immediately available for the Scout ST-6 launch. In addition, the replacement of the payload with a complete backup payload would require several days, thus delaying the launch and increasing the cost of the launch operations.

L-64-3081

(b) Completely contained within heat shield.

Figure II-16.- Concluded.

Launch Operations.- Near the end of the launch countdown the vehicle was positioned for launch (fig. II-19). At the end of the launch countdown the first stage was ignited at 18:29:44 hours and the Scout vehicle rose from its launch tower (fig. II-20) with the guidance and control system programed to fly the prescribed ascent trajectory. After first-stage burnout at an altitude of about 55,000 feet, the vehicle coasted to about 130,000 feet with first stage attached in order to provide aerodynamic stability and to minimize aerodynamic heating loads. At about 130,000 feet, the second stage was ignited and separated from the first stage. Second-stage burnout occurred at an altitude of about 260,000 feet and the drag-fairing heat shield around the third-stage rocket motor was jettisoned. The second stage with upper stages coasted to about 350,000 feet where third-stage ignition took place, and the second stage was separated. At third-stage ignition, the fourth-stage payload drag-fairing heat shield was jettisoned. It was not possible to jettison the fourth-stage payload heat shield below 350,000 feet since calculations indicated that aerodynamic heating might be seriously detrimental to experiments onboard the spacecraft. When the fourth-stage payload heat shield jettisoned, the spacecraft antennas erected. The fourth stage and the burnt-out third stage with its control and guidance system still operating coasted to the apogee of the ascent trajectory. The stages were alined to about 0.13° with the local horizon; the fourth stage was spun up to about 190 rpm by spin rockets, ignited, and blast separated from the third stage. The velocity increment gained during fourth-stage burning was sufficient to place the spacecraft into orbit. A sequence of events from launch showing pertinent events is shown in table II-2.

SECTION III - ASCENT PERFORMANCE

Preliminary analysis of telemetry and tracking radar data immediately after launch indicated nominal performance up to fourth-stage ignition and that the ascent trajectory was very close to the predicted trajectory. However, it was not possible to determine the injection point exactly since radar data obtained beyond fourth-stage ignition were questionable and flight records were not obtained beyond fourth-stage ignition since the launch vehicle telemetry systems

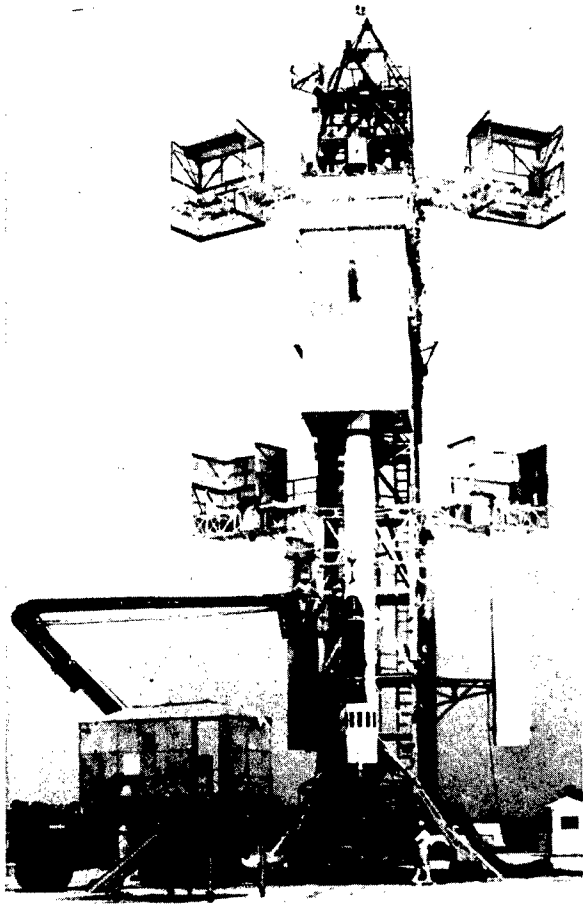

L-64-3082
Figure II-17.- Spacecraft (within fourth-stage heat shield) being elevated for assembly with launch vehicle.

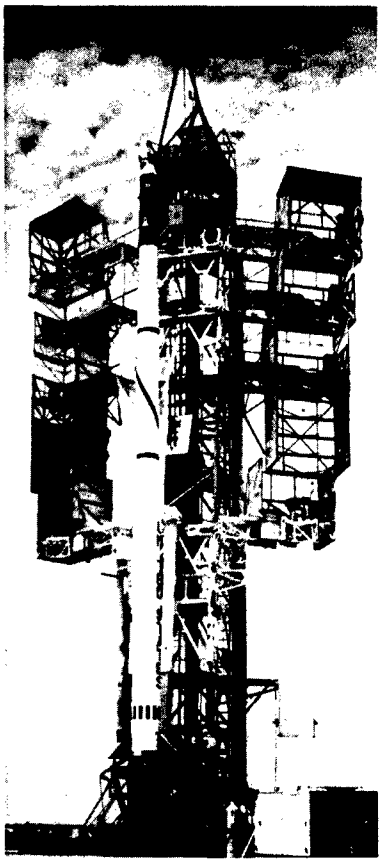

L-64-3083
Figure II-18.- Spacecraft (within fourth-stage heat shield) assembled to launch vehicle.

were located in the third stage. On this basis injection conditions were derived from subsequent Minitrack data on spacecraft position, extrapolated backward to the injection point.

In order to obtain a comparison of the actual ascent trajectory with the predicted, and with a calculation based on actual rocket performance, it was necessary to perform a postflight trajectory calculation on a digital computer by using the first- and second-stage motor performance based on accelerometer data and nominal third-stage data in place of motor performance obtained from flight records since a cursory analysis of all flight data indicated that the performance data for the third-stage motor, derived from accelerometers, was in error. Fourth-stage nominal performance was used in this calculation.

A comparison of the actual ascent trajectory as determined by radar with preflight as well as postflight calculations is presented in figure II-21. It is seen that the postflight calculation agrees well with the radar data through

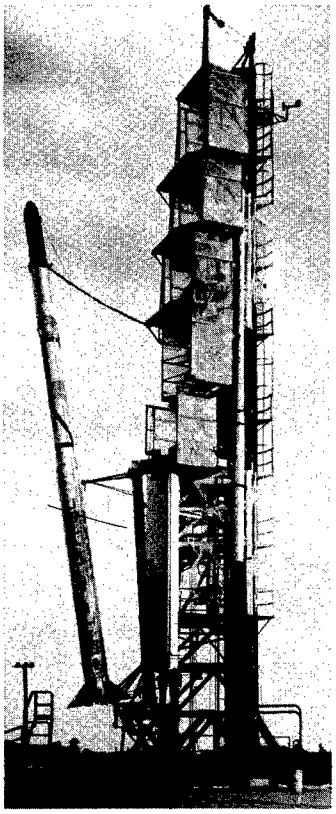

L-64-3084
Figure II-19.- Vehicle in launch attitude.

fourth-stage ignition. As stated previously, Minitrack data were used to determine injection. The difference in injection altitude as shown by the preflight and postflight calculations was about 6 nautical miles.

A comparison of the actual ground track with the predicted trajectory indicates that the vehicle followed the predicted path within about 1°. This comparison is shown in figure II-22.

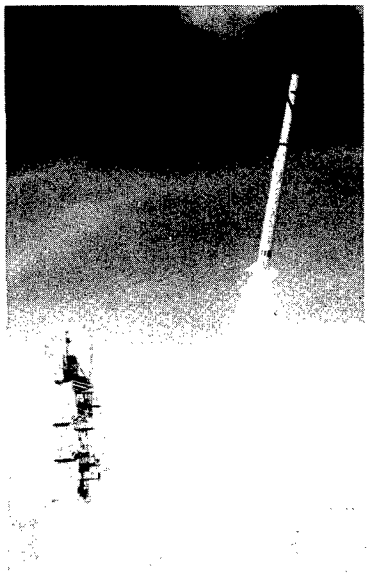

L-64-3085
Figure II-20.- Launching of spacecraft.

An analysis of the telemetered pitch-rate gyroscope output was undertaken to determine whether the pitch attitude of the vehicle varied as programed with time along the trajectory. This analysis indicated that the pitch rate did not go to zero at T + 222 seconds as programed, but continued at a negative rate of approximately 0.04 deg/sec. This amount of drift resulted in an attitude error of -11.1° at fourth-stage ignition. A trajectory computed with this pitch program resulted in an injection altitude of 246.05 nautical miles and a flight-path angle of -4.396°. These values are in close agreement with the values derived from Minitrack data. A comparison of injection conditions as determined by preflight as well as postflight calculations and derived from Minitrack data are presented in table II-3 (see ref. II-2).

SECTION IV - ORBITAL PERFORMANCE

As indicated in the previous section, a preliminary analysis of the flight data indicates that the actual vehicle trajectory appeared to be very close to the predicted trajectory. Indications were that a satisfactory orbit had been achieved. However, postflight calculations of orbital parameters based on Minitrack data revealed that the desired orbit was not achieved. Due to the previously mentioned flight-path error, the perigee was about 61 nautical miles, and the satellite, designated Explorer XIII, remained in orbit approximately $2\frac{1}{2}$ days instead of the predicted minimum of 1 year.

A comparison of the predicted orbital parameters with those obtained from Minitrack data is shown in table II-4.

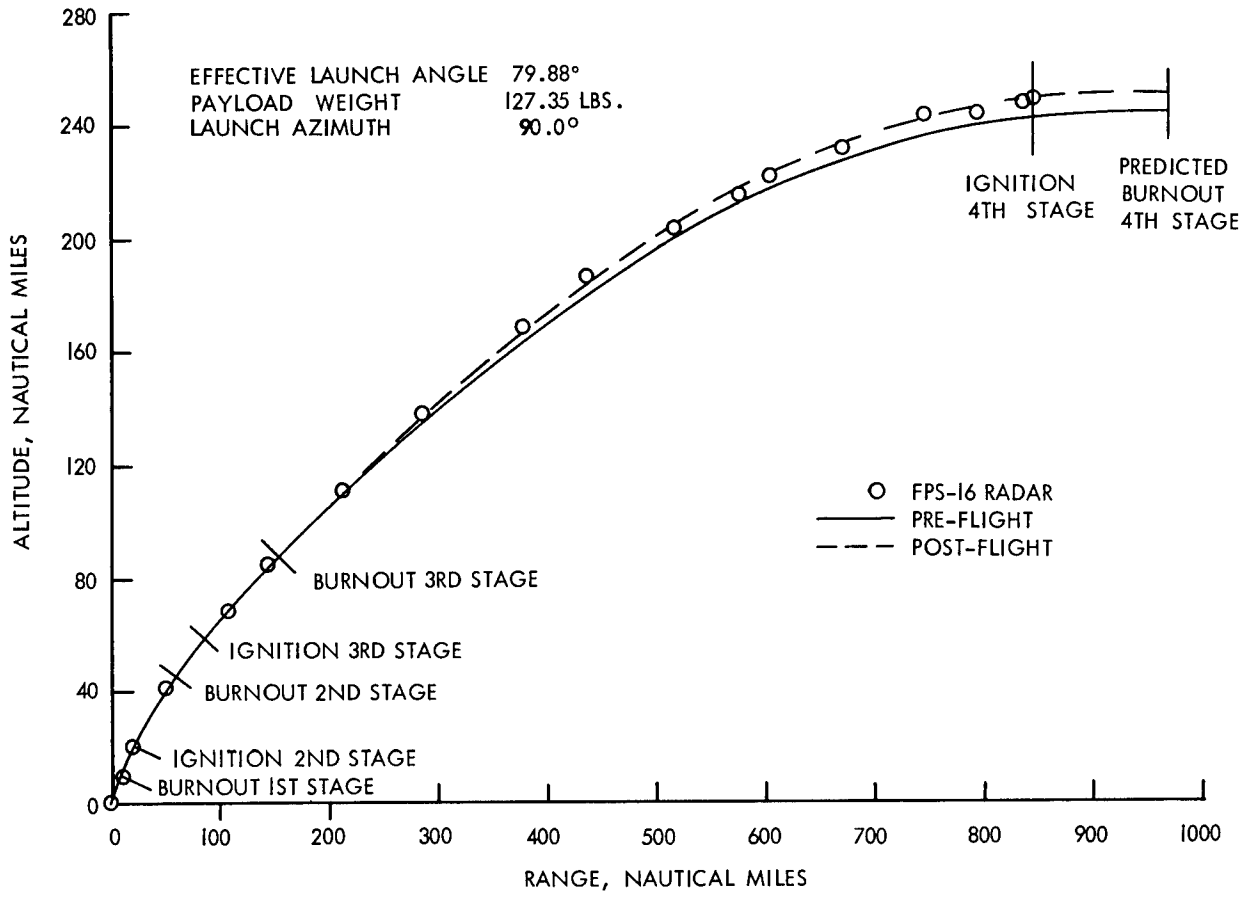

Figure II-21.- Ascent trajectory profile.

SECTION V - DATA ACQUISITION

Data acquisition from the Explorer XIII was the responsibility of the Goddard Space Flight Center, and the Minitrack Receiving Station Network had the specific responsibilities for acquiring the telemetered data. Data were received and recorded by the following stations:

Antofagasta, Chile	Lima, Peru
Blossom Point, Maryland	San Diego, California
Fort Myers, Florida	Woomera, Australia
East Grand Forks, Minnesota	Quito, Ecuador
Johannesburg, South Africa	Santiago, Chile

Acquisition of the data was accomplished in the following manner: During each period when data acquisition was required, the designated telemetry station commanded the data read-out from the Explorer XIII. Actually, since the satellite did not achieve the predicted orbit, the two telemeters were commanded whenever possible. Upon a successful interrogation, the signals from the two

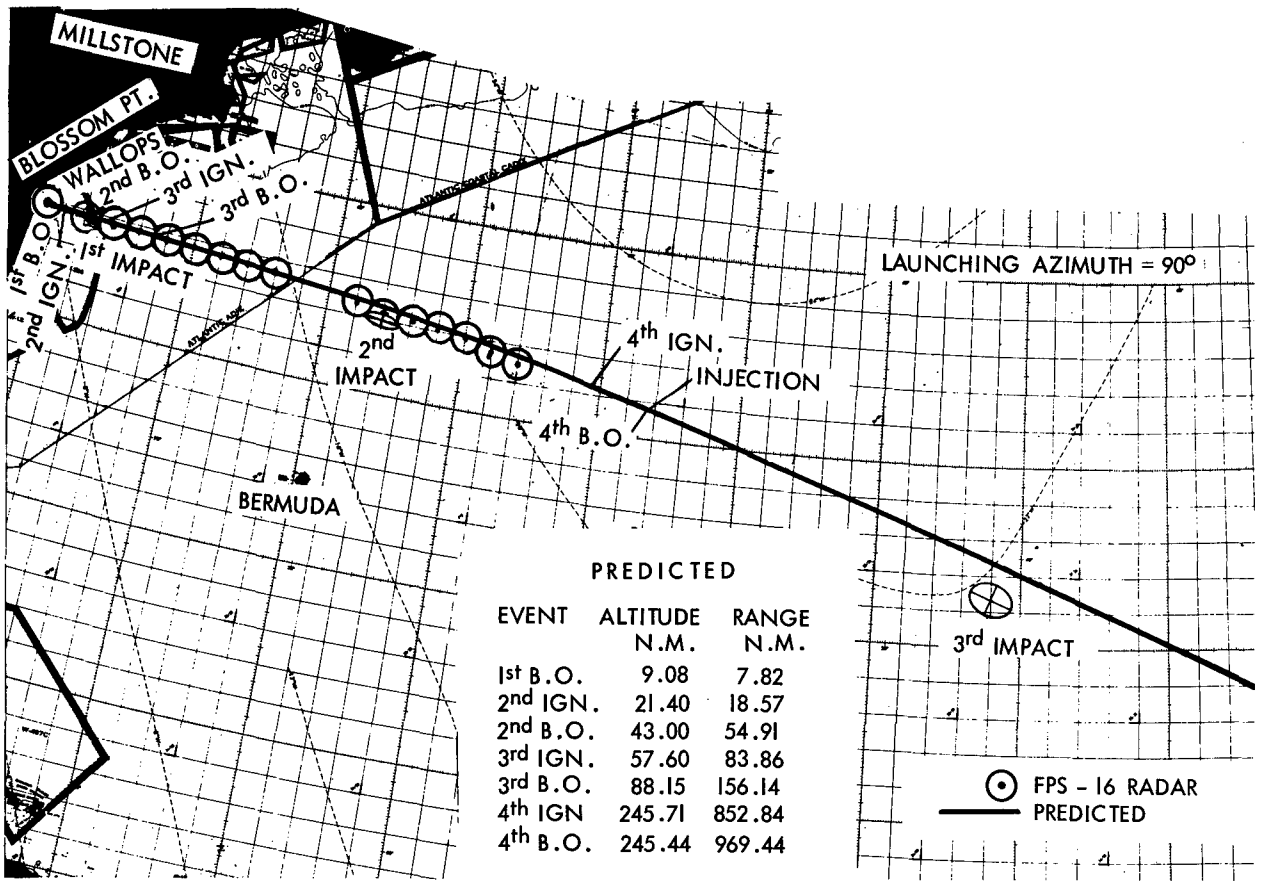

Figure II-22.- Ground track during ascent.

satellite telemeters were acquired by a circularly-polarized 136-mc antenna and fed from a pole-mounted preamplifier to a hybrid power divider. The outputs from the power divider were then separately fed to two telemetry receivers, tuned to 136.860 mc and 136.200 mc, respectively. The signals were amplitude demodulated in the receivers, with the detected outputs fed from their respective video amplifiers to a seven-channel tape recorder. At the same time that the detected signals were being recorded, the AGC (automatic gain control) level from one receiver, a 10-kc reference signal, and the Minitrack time code were also recorded.

Presented in table II-5 is a listing of the telemetry acquisitions made from the Explorer XIII from which data were obtained. Several interrogations were unsuccessful. The failure to receive data during several passes can be attributed to the rapidly decaying orbit and not knowing exactly when the satellite would be in position to be interrogated.

In addition to telemetry data acquisition, the Minitrack Network was responsible for satellite tracking. A total of 105 beacon signal acquisitions of the Explorer XIII were made.

The telemetry data received were recorded on magnetic tapes and these tapes were forwarded directly from the receiving station to the Langley Research Center for data reduction.

The telemeter receiving station set up at the launch site for final check-outs was also used to receive signals from the satellite during the first few orbits. Although the satellite was not commanded from Wallops, the radio beacon was monitored. When either Blossom Point or Fort Myers did transmit command signals, the data were received and recorded at Wallops. A photograph of the receiving station at Wallops is shown in figure II-23. In addition to an automatic tracking antenna, a manually operated antenna was used.

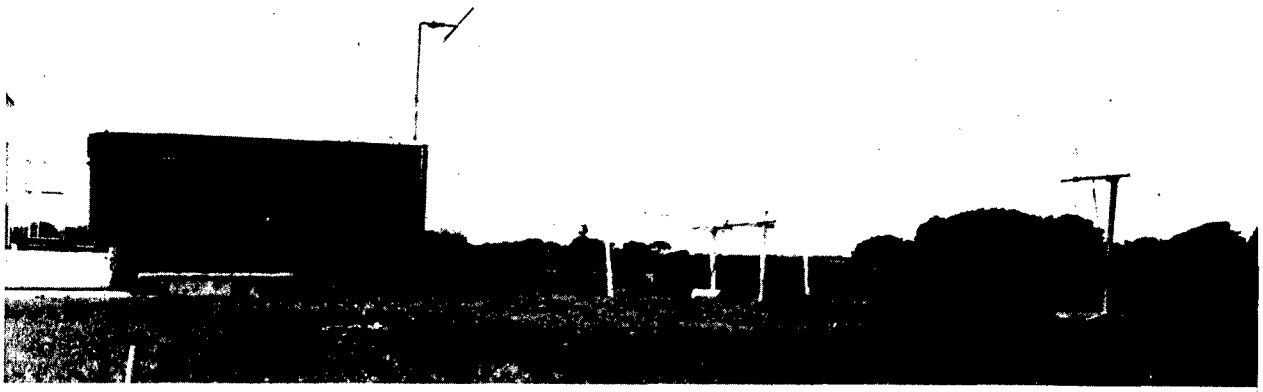

Figure II-23.- Wallops Island telemeter receiving station. L-64-3086

SECTION VI - REFERENCES

II-1. Staff of the Lewis Research Center: Micrometeoroid Satellite (Explorer XIII) Stainless-Steel Penetration Rate Experiment. NASA TN D-1986, 1963.

II-2. Freudenberger, O. L., and Devoll, J. W.: Scout ST-6, Final Flight Report. Vought Astronautics Report No. AST/EIR-23.3, 12 Oct. 1961.

TABLE II-1.- SATELLITE WEIGHT BREAKDOWN

Component	Weight, lb
Forward shell: including sounding boards, power solar-cell trays, test solar-cell trays, heat-transfer ring, antennas, Cd-S cell experiment, mounting hardware, and wiring	27.90
Bulkhead assembly: including two 48-channel telemeters, plugs, and wiring	33.93
Pressurized-cell detector: including 160 cells at 0.137 lb each, mounting hardware, plugs, and wiring	47.98
Copper-wire-card detector: including mounting hardware	4.78
Steel-covered-grid detector: including mounting hardware	6.50
Payload support	4.37
Heat-shield bumper ring and balance weights	1.89
Total payload	127.35
Spent rocket motor	47.85
Spent spin motors	1.52
Upper "D" section	13.16
Total satellite	189.88

TABLE II-2.- SEQUENCE OF EVENTS

Time, sec	Event
0.00	First-stage ignition.
42.04	First-stage burnout.
74.16	Second-stage ignition; first-stage separation.
116.96	Second-stage burnout; third-stage rocket-motor fairing separation.
135.71	Third-stage ignition; second-stage separation; fourth-stage fairing separation; antennas erected.
172.11	Third-stage burnout.
482.19	Fourth-stage spinup.
484.04	Fourth-stage ignition; third-stage separation.
525.41	Fourth-stage burnout. Injection into orbit.

TABLE II-3.- COMPARISON OF INJECTION CONDITIONS

Injection condition	Minitrack data	Preflight calculations	Adjusted postflight
Altitude, nautical miles	246.466	244.84	246.05
Inertial velocity, ft/sec	25,381.1	25,539.5	25,260.4
Flight-path angle, deg	-3.987	-0.013	-4.396
Inertial heading, deg	102.352	103.388	103.554
Latitude, deg	35.885	35.739	35.637

TABLE II-4.- COMPARISON OF ORBITAL PARAMETERS

Parameter	Minitrack data	Predicted
Apogee altitude, nautical miles	619.4	529.2
Perigee altitude, nautical miles	60.93	244.4
Orbital period, min	97.247	99.061
Eccentricity	0.073786	0.037132
Inclination, deg	37.68	37.68
Argument of perigee, deg	180.9	108.35

TABLE II-5.- ORBITAL TELEMETRY HISTORY

Orbit	Date/Time	Minitrack station	Tape	Telemeter	Data-reduction process
Launch	25/18:29:44	Blossom Point	122A001	None	None
1	25/20:11:45	Grand Forks	122N001	B	Automatic
1	25/20:11:45	Blossom Point	122A002	B	Automatic
1	25/20:17:14	Blossom Point	122A002	A	Manual*
2	25/21:59:40	Fort Myers	122D001	None	None
7	26/06:34:00	Santiago	122J001	None	None
8	26/08:32:15	Santiago	122J001	None	None
9	26/10:02:40	Antofagasta	122H001	A	Manual
9	26/10:02:40	Antofagasta	122H001	B	Manual
10	26/11:46:00	Quito	122F001	A	Manual
10	26/11:55:00	Quito	122F001	B	Manual
13	26/15:13:30	Fort Myers	122D001	A	Automatic
13	26/15:15:02	Fort Myers	122D001	B	Automatic
13	26/15:13:30	Blossom Point	122A003	A	Automatic
13	26/15:15:02	Blossom Point	122A003	B	Automatic
14	26/16:58:06	Blossom Point	122A004	A	Automatic
14	26/16:58:06	Blossom Point	122A004	B	Automatic
14	26/16:58:06	Fort Myers	122D002	A	Automatic
14	26/16:58:06	Fort Myers	122D002	B	Automatic
15	26/18:40:57	Fort Myers	122D002	A	Automatic
15	26/18:40:57	Fort Myers	122D002	B	Automatic
20	27/03:03:00	Santiago	122J002	A	Manual
20	27/03:03:00	Santiago	122J002	B	None
21	27/04:45:56	Santiago	122J003	A	Automatic
21	27/04:45:56	Santiago	122J003	B	Automatic
22	27/06:21:30	Santiago	122J003	A	Automatic
22	27/06:21:30	Santiago	122J003	B	Automatic
23	27/08:03:14	Antofagasta	122H001	A	Automatic
23	27/08:03:14	Antofagasta	122H001	B	Automatic
25	27/11:15:40	Lima	122G01	None	None
27	27/14:03:00	Woomera	122-1	None	None
28	27/15:42:15	Woomera	122-1	A	Automatic
28	27/15:42:15	Woomera	122-1	B	Automatic
35	28/02:00:03	Antofagasta	122H001	A	Manual**
35	28/02:00:03	Antofagasta	122H001	B	Manual**
40	28/08:46:00	Antofagasta	122H001	B	Manual**

*Special process by GSFC.

**The temperatures of all systems had increased beyond design limits as a result of aerodynamic heating so that these data could not be used.